Journal of Applied Polymer Science

Electrical, thermal, and viscoelastic properties of graphene nanoplatelet/poly(butylene adipate-*co*-terephthalate) biodegradable nanocomposites

Sima Kashi, Rahul K. Gupta, Nhol Kao, Sati N. Bhattacharya
Rheology and Materials Processing (RMPC) Centre, School of Engineering, RMIT University, Melbourne, Victoria 3000, Australia
Correspondence to: R. K. Gupta (E-mail: Rahul.gupta@rmit.edu.au)

ABSTRACT: Graphene nanoplatelets (GNPs) were dispersed in poly(butylene adipate-*co*-terephthalate) (PBAT) by melt-blending. Scanning electron micrographs showed good dispersion of GNPs in PBAT at low concentrations while at higher loadings, the platelets became physically in contact forming conductive pathways. Electrical conductivity of PBAT was enhanced markedly with GNP addition with a distinctly faster rate for GNP loadings higher than 6 wt % because of formation of conductive networks. Interestingly, thermal stability of PBAT was also found to increase for GNP loadings above 6 wt %. Dynamic viscoelastic properties of the nanocomposites exhibited significant enhancement with increasing GNPs. In particular, storage modulus showed less frequency dependency in the low frequency region leading to a percolation threshold of between 6 and 9 wt %, above which time–temperature superposition principle failed. Steady shear measurements revealed that GNP incorporation increased the zero-shear viscosity markedly and intensified the shear thinning behavior. Carreau model well described the shear viscosity of all the compositions. © 2016 Wiley Periodicals, Inc. J. Appl. Polym. Sci. **2016**, *133*, 43620.

KEYWORDS: biodegradable; composites; graphene; thermogravimetric analysis (TGA); viscosity and viscoelasticity; poly(butylene adipate-co-terephthalate)

Received 13 January 2016; accepted 9 March 2016
DOI: 10.1002/app.43620

INTRODUCTION

With the increasing volume of plastic wastes in landfills and sites, which has raised global concerns for protection of the environment from persistent commercial polymers (i.e., polyethylene, polypropylene, and polystyrene), moving towards environmental-friendly materials is inevitable. Poly(butylene adipate-*co*-terephthalate) (PBAT) is a completely biodegradable aliphatic/aromatic copolyester (Figure 1) derived from petroleum, which is synthesized by esterification of 1,4-butanediol with aromatic dicarboxylic acid followed by polycondensation with succinic acid.[1] It exhibits high elasticity, wear, and fracture resistance[2] as well as adhesion and compatibility with many other natural polymers.[3] In spite of its excellent properties such as very high ultimate elongation and thermal stability at elevated temperatures, PBAT has been mostly investigated in mixture with other polymers (i.e., polylactide) for production of new polymer blends.

Some researchers, however, performed studies on PBAT as the sole polymeric matrix for preparation of new materials. It has been demonstrated that incorporation of nano-sized fillers into PBAT can overcome its shortcomings such as low strength, conferring multifunctional enabling properties like enhanced mechanical, thermal, magnetic, and electrical properties.[4–8] Mohanty and Nayak[5,9] studied PBAT/organically modified nanoclays nanocomposites. Someya *et al.*[7] focused on the relationship between the morphology and tensile properties of PBAT/Montmorillonite nanocomposites. Fukushima *et al.*[10] investigated the possibility of nanocomposites based on PBAT and different clays for medical applications. Wu[6] studied the chemical and mechanical properties of PBAT/multi-walled carbon nanotubes composites. Feng *et al.*[4] investigated the crystallization and creep of PBAT/graphite nanosheets composites. Mittal *et al.*[8] studied PBAT/graphene (up to 5 wt %).

Graphene nanoplatelets (GNPs) are graphitic nanoparticles with layered structure which are composed of stacked 2D graphene sheets bonded together with weak Van der Waals forces.[11] With excellent physical properties,[12] graphene can be used for reinforcing polymers and developing novel materials with multifunctional properties[13] such as electrical conductivity which could be exploited in different areas including electrostatic discharge protection, lightening-protection panels, and electromagnetic interference shielding applications.[14–16] High-purity GNPs can be derived from the plentiful resource of natural graphite by relatively convenient approaches compared to other carbon

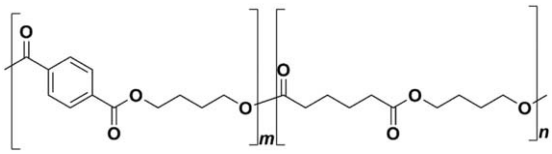

Figure 1. Chemical structure of PBAT.

nanofillers such as carbon nanofibers and nanotubes which require complex and expensive methods. GNPs are cost-effective nanofillers with potential to replace high-priced carbon nanotubes in many applications.[11,17] As a result, graphene has generated an ever increasing interest in both academia and industrial world and many researchers have started to use graphene for production of new nanocomposites.[18–27]

The present study is concerned with preparation and characterization of biodegradable PBAT/GNP nanocomposites containing 0–15 wt % (0–9.1 vol %) of GNPs. To the best of our knowledge, there has been no study on the melt flow behavior and viscoelastic properties of PBAT nanocomposites with GNP loading as high as 15 wt %. Variations of the dynamic and steady shear rheological properties of PBAT with GNP concentration are investigated in detail in the current paper. Moreover, effects of GNP reinforcement on thermal stability and electrical conductivity of the matrix are also evaluated. Dispersion state of the platelets in the polymeric matrix was examined via morphological studies, as well.

EXPERIMENTAL

Materials

PBAT (Ecoflex F Blend C1200) was purchased from BASF (Germany) with a density of 1.25–1.27 g/cm^3 and a melting temperature range of 110–120 °C.[28] GNPs were obtained from XG Sciences (USA, Michigan). The GNP grade used for this study was "M" with average thickness of 6–8 nm, surface area of 120–150 m^2/g, density of 2.2 g/cm^3, and electrical conductivity of 10^2 and 10^7 S/m perpendicular and parallel to the surface, respectively.[29]

Nanocomposites Preparation

PBAT pellets and GNPs were dried at 60 °C and 80 °C respectively for 12 hours in an oven prior to the processing. PBAT/GNP nanocomposites were prepared in an internal mixer (Haake Rheomix OS R600) with roller rotors. Mixing was performed at 140 °C (about 20 °C above the melting range of PBAT), rotor speed of 60 rpm and a mixing time of 10 minutes. A total of 60 g material was fed to the mixer for every batch. Nanocomposites were prepared with six different GNP concentrations from 0 to 15 wt %. Table I summarizes the compositions of the samples and their corresponding codes. The prepared nanocomposites were then compression moulded into 2-mm-thick circular plaques with 25-mm diameter. The compression moulding temperature was 140 °C and the compression force was kept at 80 kN for 5 min. Cooling water was then used to cool the moulding press to 50 °C.

Scanning Electron Microscopy

Neat PBAT and PBAT/GNP nanocomposites were fractured after keeping them in liquid nitrogen for 3 minutes. Samples were then sonicated in ethanol for 30 seconds and dried in a vacuum oven at 50 °C overnight prior to the microscopy. Fractured surface morphology of the samples was studied using a FEI Quanta 200 scanning electron microscope. For samples with up to 6 wt % GNPs, an accelerating voltage of 5 kV was employed to avoid charging and for nanocomposites with higher GNP concentrations, accelerating voltage was fixed at 10 kV.

Thermogravimetric Analysis

The thermal decomposition characteristics of PBAT/GNP nanocomposites were measured by a thermal gravimetric analyzer (STA 6000, Perkin Elmer). Samples were first stabilized at 50 °C for 2 minutes and then heated up to 900 °C under a nitrogen atmosphere at a heating rate of 10 °C/min.

Electrical Conductivity

A vector network analyzer (Wiltron 37269A) with waveguide setup was used to measure the scattering parameters of PBAT/GNP nanocomposites over the frequency range of 8.2–12.4 GHz (X-band). Electrical permittivity of the nanocomposites was extracted from the scattering parameters according to Nicolson–Ross–Weir (NRW) method.[30] AC conductivity was then determined from permittivity.

Melt Rheology

Dynamic and steady shear rate rheology of the PBAT/GNP nanocomposites was assessed using a strain-controlled Advanced Rheometrics Expansion System (ARES) rheometer (TA Instruments) with a force transducer of torque range of 0.2–200 g.cm and parallel-plate fixture of 25 mm diameter. Measurements were performed at 140 °C. Linear viscoelastic region of each PBAT/GNP composition was first determined by running strain sweep tests at an angular frequency of 10 rad/s and strain range of 0.034–270%. Frequency sweeps were then conducted on fresh samples within their linear region to determine the effect of GNP concentration on storage and loss moduli and also complex viscosity of PBAT. Steady shear rate experiments were conducted for each sample over the shear rate range of 0.01 to 4 s^{-1}. At higher shear rates slip occurred.

RESULTS AND DISCUSSION

Morphology

Figure 2 shows the micrographs of PBAT/GNP nanocomposites. It is observed that at low GNP concentration of 3 wt %, the graphene platelets are well dispersed in the matrix and PBAT chains have separated the platelets. For nanocomposite with 6 wt % of nanofiller, in addition to the separated platelets some chunks of GNPs can also be seen while they are still separated from each other by PBAT. As the GNP concentration is raised to 9 wt %, a higher degree of GNP agglomeration is observed and the platelets and agglomerates become physically in contact with one another. The formation of this GNP network throughout the polymer matrix at 9 wt % GNPs was also detected by the sharp increment in the electrical conductivity at this filler

Table I. Composition of PBAT/GNP Nanocomposites

Sample codes	PB0	PB3	PB6	PB9	PB12	PB15
PBAT (wt %)	100	97	94	91	88	85
GNPs (wt %)	0	3	6	9	12	15

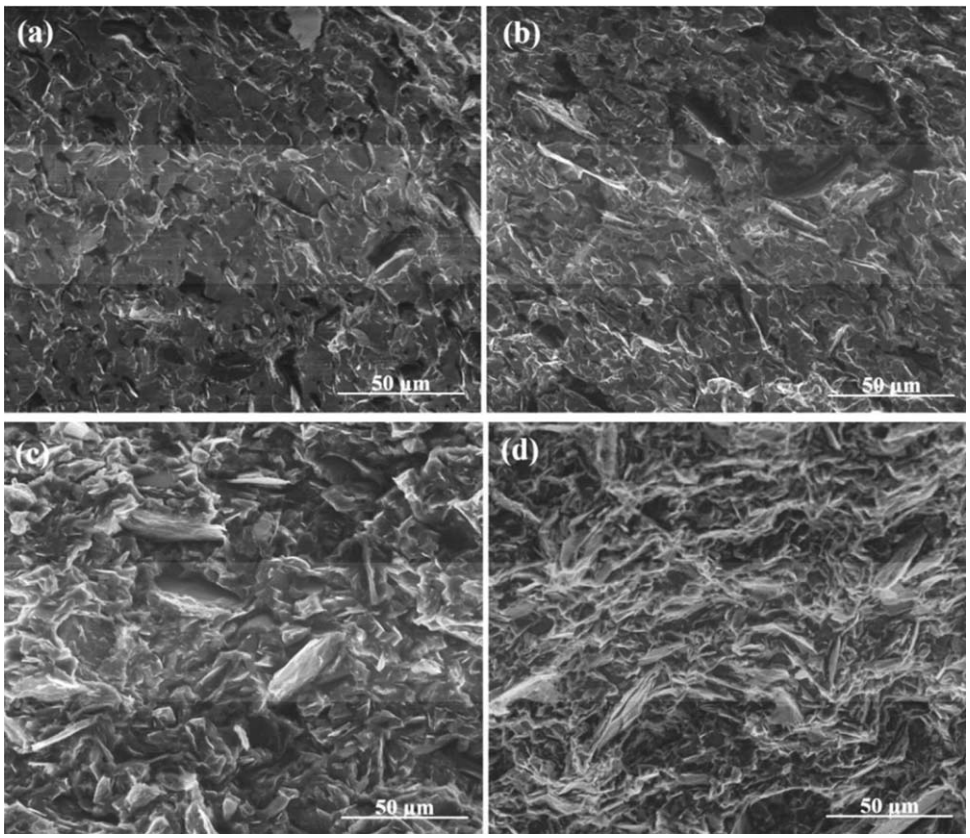

Figure 2. SEM images of PBAT/GNP nanocomposites with (a) 3, (b) 6, (c) 9, and (d) 12 wt % GNPs.

loading (next section). At 12 wt %, GNPs are very densely positioned in PBAT with their agglomerates forming an interconnected 3D network within the matrix. The nanocomposite with 15 wt % of GNPs was observed to have morphology very similar to that of PB12 and therefore is not demonstrated here. The high degree of GNP agglomeration and incapability of polymer to separate the platelets at high GNP loadings has been observed by other researches as well. In a study performed on poly (propylene)/GNP nanocomposites, Li *et al.*[31] reported the separation of GNPs at 5 wt % while at 15 wt %, the platelets formed agglomerates and became in contact. Narimissa *et al.*[32] and Kashi *et al.*[33] also observed high degree of agglomeration and tactoid formation at high levels of GNP loadings in different grades of poly lactide.

Electrical Conductivity

Figure 3 displays the AC conductivity of PBAT/GNP nanocomposites as a function of GNP loading. Pristine PBAT has a conductivity of about 0.11 S/m which increases to more than 3 S/m with addition of 15 wt % GNPs. An interesting observation made in Figure 3 is that with increasing GNP concentration from 0 to 6 wt %, conductivity increases gradually but as the GNP loading is increased further, a sharper increase is observed which is confirmed by the change in slope which occurs. This sharp increase in electrical conductivity occurring as the GNP concentration is raised above 6 wt % is associated with the formation of electrically conductive pathways of GNPs. At low loadings, the nanoplatelets are separated from each other by PBAT chains as was observed in Figure 2. By increasing the GNP content above the percolation threshold, the graphene platelets are positioned more closely in PBAT and establish physical contact with each other and therefore an electrically conductive network is formed in the matrix, which enhances the conductivity of the nanocomposites significantly.

Thermal Stability

Thermal stability is an important parameter for polymeric materials since it could be a limiting factor in processing as well as in end-use applications.[34] Thermogravimetric analysis (TGA) curves of PBAT/GNP nanocomposites are presented in Figure 4

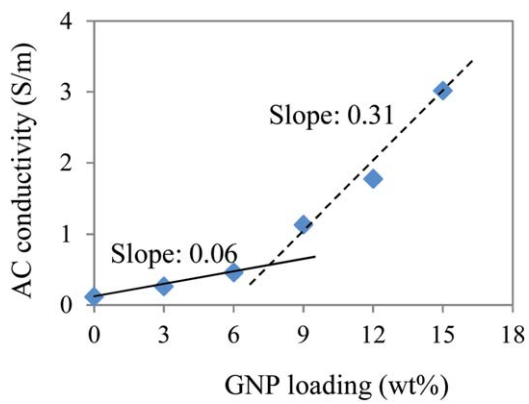

Figure 3. AC conductivity of PBAT/GNP nanocomposites versus GNP loading at 10 GHz. [Color figure can be viewed in the online issue, which is available at wileyonlinelibrary.com.]

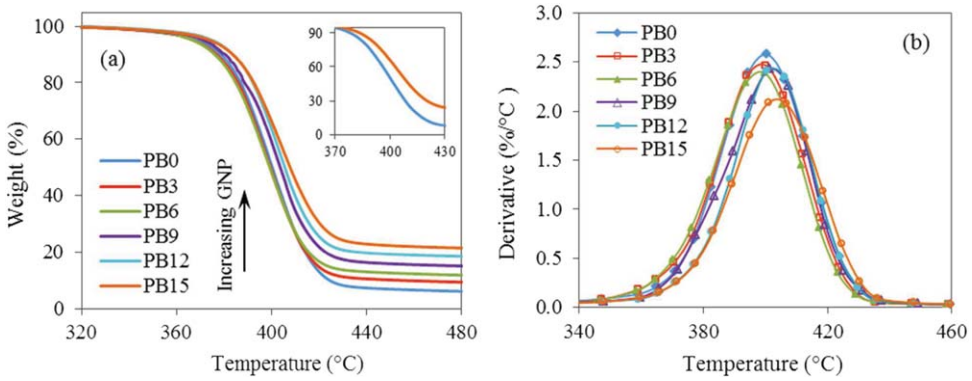

Figure 4. (a) TGA curves and (b) weight loss rate curves of neat PBAT and PBAT/GNP nanocomposites under nitrogen and at a heating rate of 10 °C/min. [Color figure can be viewed in the online issue, which is available at wileyonlinelibrary.com.]

and the temperatures of samples at which 5%, 10%, and 50% weight losses occur are summarized in Table II ($T_{5\%}$, $T_{10\%}$, and $T_{50\%}$). It is observed that the thermal degradation of neat PBAT and PBAT/GNP nanocomposites takes place as a single step process. The onset thermal degradation of pristine PBAT is detected to be 338 °C (1% weight loss) and the degradation is completed at 426 °C leaving an ash content of about 5% at the end of the test. It is evident from Figure 4(a) that addition of GNPs up to 6 wt % does not alter the thermal stability of the matrix considerably. However, as the GNP concentration is raised above 6 wt % to 9 wt % and higher, nanocomposites exhibit enhanced thermal stability with their TGA curves being gradually shifted towards higher temperatures. This can clearly be seen in the inset plot of Figure 4(a) which compares the TGA curves of pure PBAT and PB15. While the onset degradation temperature of PB15 is only 2 °C higher than that of pure PBAT, the effect of GNPs is more pronounced at higher weight losses. As it can be seen from Table II, $T_{5\%}$ and $T_{50\%}$ increase by 5 °C and 7 °C as the GNP loading is increased from 0 to 15 wt %. This delay in thermal degradation of PBAT could be attributed to the shielding effect conferred by the flake-like shape of GNPs, which hinders the diffusion of volatile decomposition products within the nanocomposites.[34,35] Figure 4(b) also shows that the temperature of the maximum weight loss rate (dm/dT_{max}) slightly shifts to higher temperatures with increasing GNP loading to 15 wt % while the maximum weight loss rate decreases by about 0.5%/°C as the GNP content is raised from 0 to 15 wt %.

Dynamic Shear Rheology

Investigating the flow behavior of polymer/nanofiller systems provides fundamental knowledge on their structure and processability. Melt rheology of these materials are influenced by their microstructure. The state of filler network in the nanocomposites can also be detected via the variation of the viscoelastic properties such as storage modulus with frequency within the linear viscoelastic region.[36] The angular frequency dependency of the dynamic storage and loss moduli of neat PBAT and PBAT/GNP nanocomposites is depicted in Figure 5. With increasing GNP loading, both moduli are enhanced over the entire frequency range. Pristine PBAT shows a typical polymer melt behavior where G' increases with increasing frequency and a clear terminal zone is observed at lower frequency region. Increasing the GNP content of the nanocomposites increases both of the moduli monotonically at high frequencies (> 10 rad/s). On the other hand, at lower frequencies, while adding GNPs up to 9 wt % slightly improves the viscoelastic properties of the matrix, above 9 wt %, the increase in the moduli particularly G' is significant. When the interactions between the anisotropic filler particles becomes significant, the system exhibits an apparent yield stress which is detected by appearance of a plateau in the dynamic moduli at low frequencies especially in G'.[37,38] The diminishing frequency dependency of G' and the appearance of a plateau in the low-frequency region for GNP concentrations above 9 wt % is indicative of formation of a percolated network within the nanocomposite, which causes the solid-like behavior (G' and $G'' \propto \omega^0$) at low frequencies.[34,36,39]

Figure 6 compares the storage moduli of neat PBAT and PBAT/GNP nanocomposites with their corresponding loss moduli. G'' of pure PBAT, PB3 (not shown here), PB6, and PB9 (not shown here) are distinctively higher than their corresponding G' over the entire frequency range. Nevertheless, at high frequencies, G' and G'' of these samples coincide with the crossover point shifting to lower frequencies as the GNP content is increased. PB12 and PB15, however, exhibit a different behavior. G' and G'' of each of these two nanocomposites have very close values with two crossover points; one at a high frequency and one at a low frequency.

Figure 7 illustrates the variations of the complex viscosities, $|\eta^*|$, of PBAT/GNP nanocomposites with frequency as a function of

Table II. TGA Analysis of Pure PBAT and PBAT/GNP Nanocomposites

Sample	$T_{5\%}$ (°C)	$T_{10\%}$ (°C)	$T_{50\%}$ (°C)
PB0	369.25	378.62	400.25
PB3	368.11	377.05	399.92
PB6	369.58	378.31	400.35
PB9	371.82	380.54	403.61
PB12	373.81	383.20	405.10
PB15	374.35	383.71	407.77

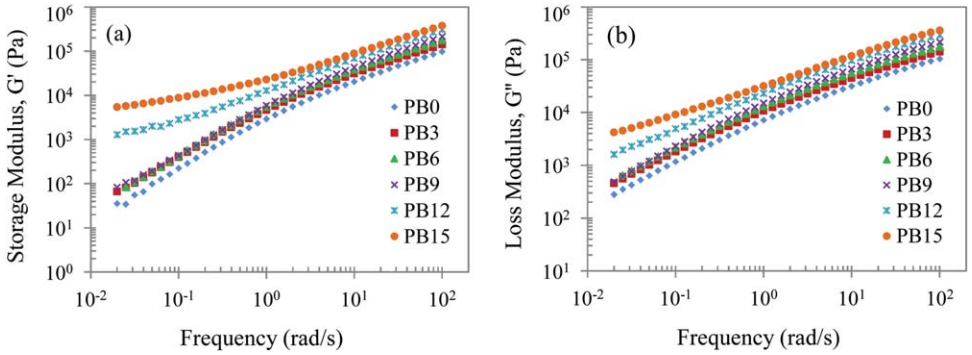

Figure 5. (a) Storage G' and (b) loss G'' moduli of neat PBAT and PBAT/GNP nanocomposites at 140 °C. [Color figure can be viewed in the online issue, which is available at wileyonlinelibrary.com.]

GNP concentration. Neat PBAT exhibits a Newtonian plateau at low frequencies and a shear thinning behavior at higher frequencies. Addition of GNPs markedly alters the flow characteristics of the matrix. The viscosity increases with GNP content. The effect of GNPs is most pronounced in the low-frequency region and decreases as the frequency is increased as a consequence of shear thinning. An interesting observation is that addition of up to 9 wt % of GNPs does not change the trend of neat PBAT flow curve and only shifts the curve upward. On the other hand, nanocomposites with 12 and 15 wt % of GNPs show not only much higher viscosities but also their flow curves have steeper slopes at low frequencies with no clear Newtonian plateau. These observations are in agreement with previously reported data on other polymer/nanofiller systems.[34,37,38,40–43] The significant enhancement in the viscosity of PBAT/GNP nanocomposites with high GNPs can be ascribed to the increased interactions between PBAT and the platelets (because of the increase in amount of the platelets) which reduce the mobility of PBAT chains, stronger interactions among the platelets themselves as their mean distance is reduced and also the formation of a network of GNPs within the matrix [as detected in Scanning Electron Microscopy (SEM) images in **Morphology** section].

The critical filler concentration beyond which the interactions between the particles become significant and a percolating 3D network is established within the matrix is said to be the percolation threshold. The effect of filler loading on G' at low frequencies can be used to predict this threshold.[39,44] Figure 8 depicts the slope of log G'–log ω at low-frequency region (α) versus GNP concentration. The sudden change in the slope is an indication of percolation threshold beyond which the liquid-like behavior is changed to the solid-like response.[39] The percolations concentration of GNPs in PBAT is found to be between 6 (3.5 vol %) and 9 wt % (5.3 vol %) at 140 °C. Note that temperature is a critical parameter affecting the percolation threshold. It is expected that by increasing the

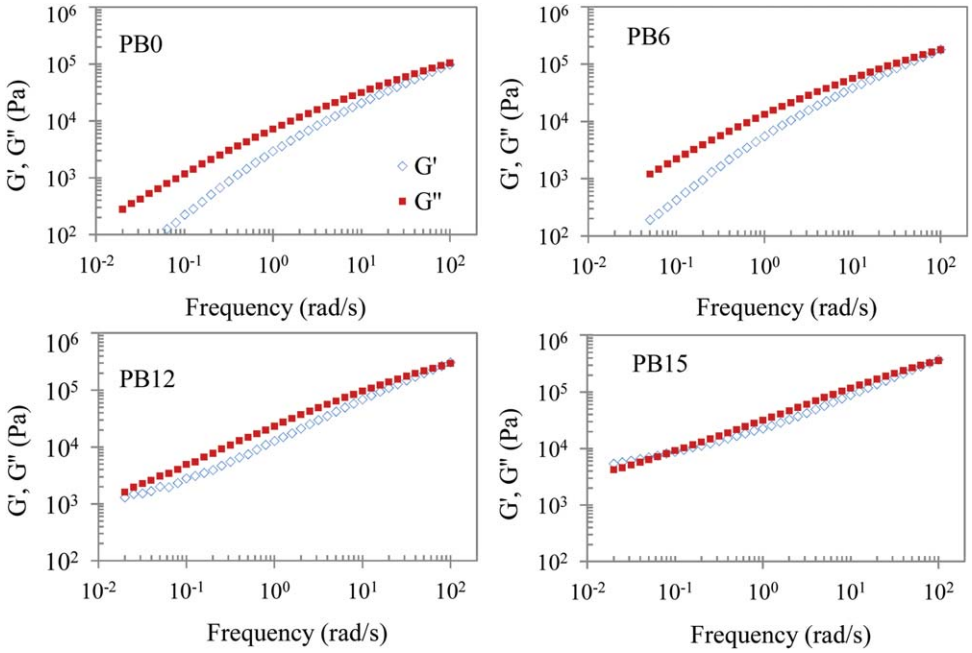

Figure 6. Comparative illustration of G' and G'' of PBAT/GNP nanocomposites. [Color figure can be viewed in the online issue, which is available at wileyonlinelibrary.com.]

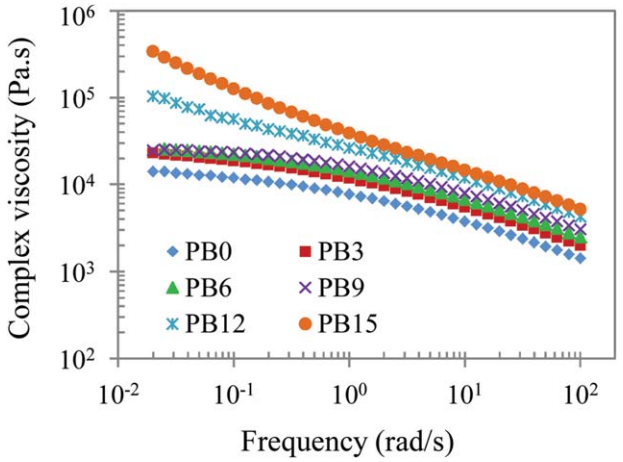

Figure 7. Complex viscosity of neat PBAT and PBAT/GNP nanocomposites at 140 °C. [Color figure can be viewed in the online issue, which is available at wileyonlinelibrary.com.]

temperature, the adsorption of polymer chains to the nanofiller interface increase, leading to a higher apparent volume fraction of the swollen particles resulting in a lower percolation threshold.[44]

Time–Temperature Superposition

For many polymers and some filled-polymer systems usually with low filler content, time–temperature superposition (TTS) principle can be applied to viscoelastic properties (i.e. storage modulus) obtained at different temperatures in order to generate a master-curve at a reference temperature that covers a wider range of frequency. Materials to which TTS is applicable are said to be thermorheologically simple. A simple and direct method for checking the applicability of TTS is to plot the loss angle versus log complex modulus (Van Grup–Palmen plot) at different temperatures.[45] If the curves superimpose, the material is thermorheologically simple. On the other hand if the curves split up, TTS will not be applicable. The Van Gurp–Palmen plots were prepared for the PBAT/GNP nanocomposites (Figure 9). TTS was found to be applicable to PBAT nanocomposites with low GNP content (0–6 wt %) while it failed for higher loadings. Thermorehological complexity has been observed for various polymer/nanofiller systems.[46–48]

At this point, it is noteworthy to mention that temperature range is also a determining factor in applying TTS. A material might follow TTS over a specific temperature range while exhibiting thermorheological complexity out of this range. For example, PB6 was found to fail the TTS as the temperature was raised from 200 °C to 220 °C at which a plateau appeared in storage modulus in the low-frequency region. This phenomenon is attributed to occurrence of physical gelation at elevated temperatures. A physical gel is considered a percolated three-dimensional network, in which physical interactions are responsible for the macroscopic connectivity.[48] It seems that at elevated temperatures, the adsorption of PBAT chains to the graphene platelets enhances. The adsorbed polymer chains not only increase the effective filler volume fraction in the system but can also function as bridges between neighboring particles (facilitating percolation).[49] These physical cross-linking interactions induced by GNPs result in the formation of a 3D network at lower filler concentrations throughout the nanocomposite leading to a solid-like behavior and deviation from TTS.

Figure 10 illustrates the master-curves of storage modulus for PBAT, PB3, and PB6 with the reference temperature being 180 °C. It can be seen that by applying time–temperature superposition, the range of angular frequency has increased from 0.05–100 rad/s to 0.03–170 rad/s.

The temperature dependence of the horizontal shift factors of pure PBAT, PB3 and PB6 were found to follow the Arrhenius relation very well:

$$a_T = \exp\left[\frac{E_a}{R}\left(\frac{1}{T}-\frac{1}{T_0}\right)\right]$$

Here T is the absolute temperature, R is the universal gas constant (8.314 J/mol), and E_a is called as the flow activation energy by analogy with reaction rate theory and is often used to characterize polymers. E_a can be obtained from the slope of $\ln(a_T)$ versus $1/T$ plot. The activation energy of PBAT was found to slightly decrease from 48.88 to 46.26 kJ/mol with increasing GNP loading from 0 to 6 wt %, respectively. Arrhenius relation implies that a material with lower E_a is less temperature sensitive. For example, for the same increase in temperature, the viscosity of a material with lower E_a decreases less compared to another material with higher E_a. The decrease in the viscosity of a polymer melt with increasing temperature is because of greater free volume available for molecular motion at higher temperatures. Therefore, since the increase in free space with temperature is limited only to the polymer fraction of a filled system, the temperature sensitivity decreases with increasing filler loading and consequently, filled polymers have lower E_a values.[50] This explains why PBAT/GNP nanocomposites have lower activation energies than pure PBAT.

Steady Shear Rheology

Figure 11 illustrates the shear rate dependency of steady shear viscosity of PBAT/GNP nanocomposites. Pristine PBAT shows a Newtonian plateau at low shear rates followed by a shear thinning behavior. While addition of 3 wt % of GNPs increases PBAT's zero-shear viscosity by 40%, shear rate dependency of PB3 remains similar to that of neat PBAT. At low shear rates,

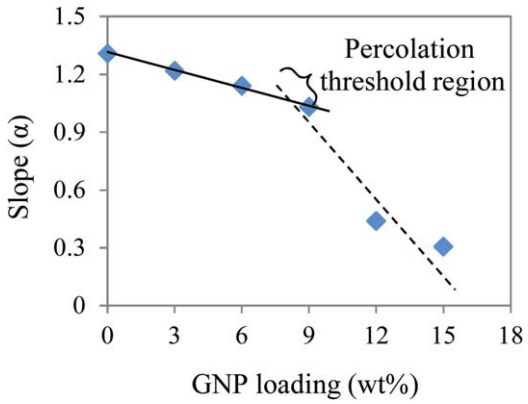

Figure 8. Slope (α) of G' versus GNP loading at 140 °C. [Color figure can be viewed in the online issue, which is available at wileyonlinelibrary.com.]

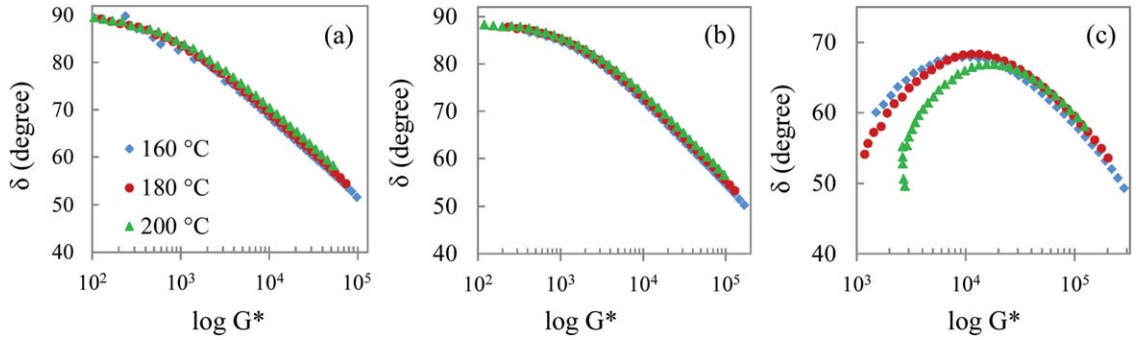

Figure 9. Loss angle (δ) versus log G^* of (a) PB0, (b) PB6, and (c) PB12. [Color figure can be viewed in the online issue, which is available at wileyonlinelibrary.com.]

shear viscosity monotonically increases with GNP content. About 100%, 205%, 365%, and 950% elevations in zero-shear viscosity were measured for PB6, PB9, PB12, and PB15, respectively. Although all the samples demonstrate shear thinning behavior at higher shear rates, the critical shear rate at which Newtonian region is intersected by shear thinning region occurs at drastically lower shear rates as the GNP content is raised above 6 wt %. The pronounced shear thinning behavior for highly filled nanocomposites may be because of the polymer imprisonment between the platelets, causing the polymer to undergo a larger effective strain rate. Moreover, the preferential orientation of GNP layers or even anisotropic tactoids parallel to the flow direction at elevated shear rates can lead to nanocomposites having viscosities comparable with or even lower than the viscosity of pure PBAT at such shear rates. Similar trends have been reported for various polymer/filler systems.[39,42,51]

To further investigate the dependency of shear viscosity of PBAT/GNP nanocomposites on the shear rate, Carreau model[52] was fitted to the data. Figure 12 compares the model predictions with experimental data. The model's parameters are the shear viscosity (η), the zero-shear viscosity (η_0), the characteristic time (λ), and n which is a dimensionless parameter indicating the slope of the curve in shear-thinning region ($0 \leq n < 1$). Values of λ and n were obtained by minimizing the root-mean-square (RMS) values. Results are summarized in Table III. With very low values of RMS for all the nanocomposites, Carreau model is found to be a good fit to the experimental data. Table III shows that characteristic time of the nanocomposites increases with increasing the GNP loading. It is also observed that the n-value decreases from 0.6 to 0.19 as the GNP concentration is increased from 0 to 15 wt %. Since the slope of viscosity versus shear rate on the bi-logarithmic plot in the power-law region is $(n-1)$, the decreasing trend of n with increasing the GNP concentration indicates the pronounced shear-thinning behavior in presence of GNPs. Similar trends have been reported for other types of nanocomposites, as well[39,42]:

$$Carreau\ model: \frac{\eta}{\eta_0} = \frac{1}{\left[1+(\lambda\dot{\gamma})^2\right]^{\left(\frac{1-n}{2}\right)}}$$

Cox–Merz Relation

Use of rotational rheometers for measuring steady shear viscosity of polymeric systems can be limiting since such rheometers are suitable for low to medium range shear rates of up to 10 s^{-1}. This is because at higher shear rates the material tends to extrude from the small gap of the plates, resulting in an inaccurate reading.[44] One of the methods to overcome this problem and estimate the viscosity at high shear rates is to use Cox–Merz rule. According to this empirical relation, the steady shear and the complex viscosities are closely comparable for the same magnitudes of shear rate and angular frequency according to the formula: $lim_{\dot{\gamma}\to\omega}\ \eta(\dot{\gamma}) = |\eta^*(\omega)|$.[41] It is observed from Figures 7 and 11 that both the steady shear viscosity and the complex viscosity of the PBAT/GNP nanocomposites decrease with increase in shear rate or angular frequency and increase with the GNP content. However, Cox–Merz equation only fitted to pure PBAT and PB3 (Figure 13). As the GNP concentration is

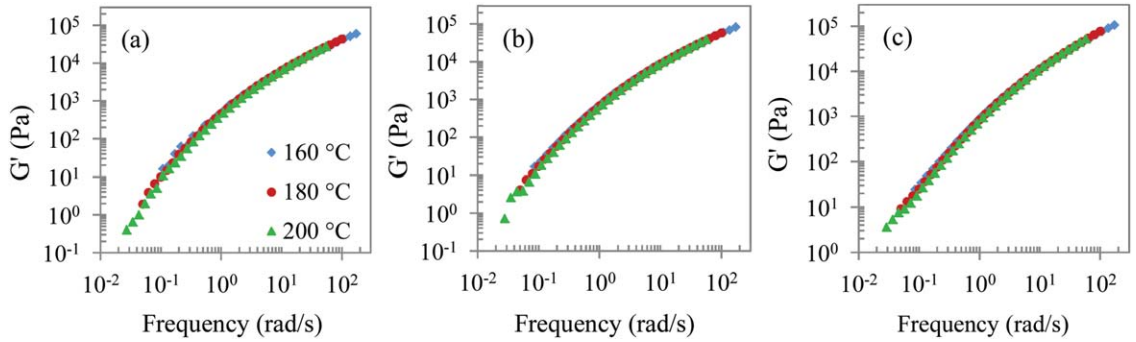

Figure 10. Storage modulus master-curves of (a) PB0, (b) PB3, and (c) PB6 (reference temperature: 180 °C). [Color figure can be viewed in the online issue, which is available at wileyonlinelibrary.com.]

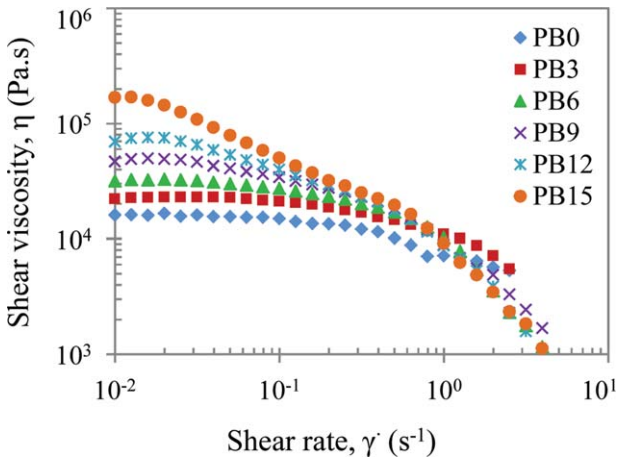

Figure 11. Steady shear viscosity of neat PBAT and PBAT/GNP nanocomposites 140 °C. [Color figure can be viewed in the online issue, which is available at wileyonlinelibrary.com.]

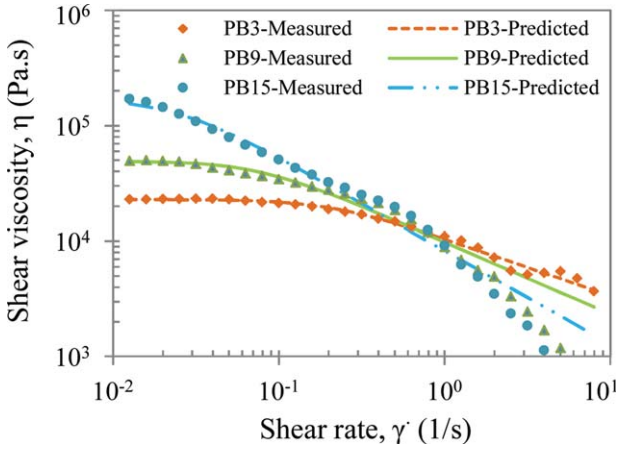

Figure 12. Comparison between measured and Carreau model predicted shear viscosity and of PBAT/GNP nanocomposites. [Color figure can be viewed in the online issue, which is available at wileyonlinelibrary.com.]

increased to 6 wt % and above, the deviation from Cox–Merz becomes more pronounced, with PB15 exhibiting a complex viscosity significantly higher than its shear viscosity. Similar observations have been reported for various filler-polymer systems with anisotropic fillers.[41,53] The failure of Cox–Merz may be a result of changes in the microstructure of the nanocomposite and some preferential orientation of highly anisotropic nanofiller because of shearing.[53]

Table III. Carreau Model Parameters of Pure PBAT and PBAT/GNP Nanocomposites

Samples	λ	n	RMS
PB0	6.36	0.60	0.026
PB3	4.82	0.51	0.020
PB6	5.21	0.21	0.051
PB9	13.18	0.37	0.045
PB12	23.35	0.35	0.034
PB15	41.66	0.19	0.030

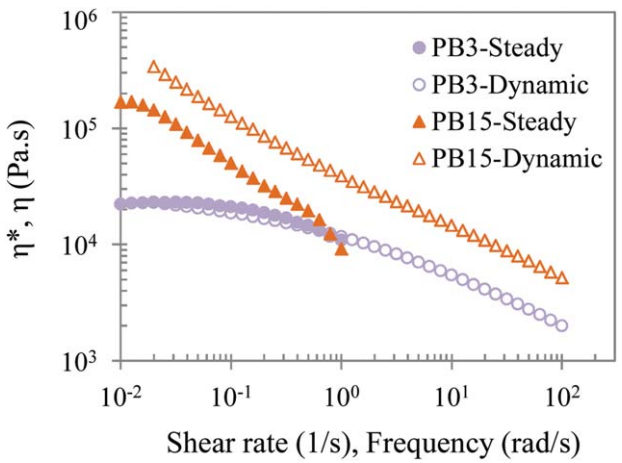

Figure 13. The steady shear viscosity (filled symbols) versus shear rate and complex viscosity (open symbols) versus frequency for PB3 and PB15. [Color figure can be viewed in the online issue, which is available at wileyonlinelibrary.com.]

CONCLUSIONS

PBAT/GNP biodegradable nanocomposites were prepared via melt mixing with 0–15 wt % (0–9.1 vol %) of GNPs. SEM micrographs showed good dispersion of the platelets at low concentrations while above 6 wt %, GNPs were found to agglomerate and become physically in contact with one another forming a 3D network within the matrix. Embedding GNPs in PBAT enhanced the low AC conductivity of the pure matrix from 0.11 to 3 S/m at 15 wt % of GNPs. At filler loadings above 6 wt %, conductivity increased at a faster rate, which confirmed the built up of conductive pathways of GNPs at high loadings detected by SEM. Nanocomposites with GNP content higher than 6 wt % also showed better thermal stability.

Addition of GNPs significantly altered the dynamic and steady shear flow behavior of PBAT. Viscoelastic properties of PBAT were enhanced with increasing GNP loading particularly in low-frequency region. Rheological percolation threshold of GNPs in PBAT was found to be between 6 and 9 wt %, which was in accordance with SEM and conductivity results. Furthermore, it was observed that above 6 wt %, time–temperature superposition was not applicable to PBAT/GNP nanocomposites. Steady shear tests also revealed the significant effect of GNPs on the shear viscosity of PBAT which increased by 950% as the GNP concentration was raised to 15 wt %. Moreover, the extent of Newtonian region decreased and a stronger shear thinning behavior was observed with increasing GNP loading. Carreau model well described the shear viscosity of the nanocomposites while Cox–Merz rule was applicable only to up to 3 wt % of GNPs.

REFERENCES

1. Hong, S. Y.; Ko, S. W.; Choi, H. J.; Lee, J. H. *J. Macromol. Sci. B* **2012**, *51*, 125.
2. Shahlari, M.; Lee, S. *Polym. Eng. Sci.* **2012**, *52*, 1420.
3. Yeh, J. T.; Tsou, C. H.; Huang, C. Y.; Chen, K. N.; Wu, C. S.; Chai, W. L. *J. Appl. Polym. Sci.* **2009**, 680.

4. Feng, S.; Wu, D.; Liu, H.; Chen, C.; Liu, J.; Yao, Z.; Xu, J.; Zhang, M. *Thermochim. Acta* **2014**, *587*, 72.
5. Mohanty, S.; Nayak, S. K. *Polym. Compos.* **2009**, 1194.
6. Wu, C. S. *Carbon* **2009**, *47*, 3091.
7. Someya, Y.; Sugahara, Y.; Shibata, M. *J. Appl. Polym. Sci.* **2005**, *95*, 386.
8. Mittal, V.; Chaudhry, A. U.; Luckachan, G. E. *Mater. Chem. Phys.* **2014**, *147*, 319.
9. Mohanty, S.; Nayak, S. K. *J. Polym. Environ.* **2012**, *20*, 195.
10. Fukushima, K.; Rasyida, A.; Yang, M. C. *Appl. Clay Sci.* **2013**, *8081*, 291.
11. Li, B.; Zhong, W. H. *J. Mater. Sci.* **2011**, *46*, 5595.
12. Hernández, M.; Bernal, M. dM.; Verdejo, R.; Ezquerra, T. A.; López-Manchado, M. A. *Compos. Sci. Technol.* **2012**, *73*, 40.
13. Martin-Gallego, M.; Bernal, M. M.; Hernandez, M.; Verdejo, R.; Lopez-Manchado, M. A. *Eur. Polym. J.***2013**, *49*, 1347.
14. Antar, Z.; Feller, J. F.; Noël, H.; Glouannec, P.; Elleuch, K. *Mater. Lett.* **2012**, *67*, 210.
15. Chen, L.; Rende, D.; Schadler, L. S.; Ozisik, R. *J. Mater. Chem. A* **2013**, *1*, 3837.
16. Fletcher, A.; Gupta, M. C.; Dudley, K. L.; Vedeler, E. *Compos. Sci. Technol.* **2010**, *70*, 953.
17. Fukushima, H.; Drzal, L. Proceedings of the 17th Annual Conference of the American Society for Composites, Purdue University, West Lafayette, IN, **2002**.
18. Liang, J. Z.; Wang, J. Z.; Tsui, G. C. P.; Tang, C. Y. *Polym. Test.* **2015**, *48*, 97.
19. Liang, J. Z.; Du, Q.; Wei, L. Y.; Tsui, C. P.; Tang, C. Y.; Law, W. C.; Zhang, S. D. *Polym. Test.* **2015**, *45*, 179.
20. He, F. A.; Wu, H. J.; Yang, X. L.; Lam, K. H.; Fan, J. T.; Chan, L. W. H. *Polym. Test.* **2015**, *42*, 45.
21. Noh, Y. J.; Kim, S. Y. *Polym. Test.* **2015**, *45*, 132.
22. Ribeiro, H.; da Silva, W. M.; Neves, J. C.; Calado, H. D. R.; Paniago, R.; Seara, L. M.; Mercês Camarano, D.; Silva, G. G. *Polym. Test.* **2015**, *43*, 182.
23. Gonçalves, V.; Brandão, L.; Mendes, A. *Polym. Test.* **2014**, *37*, 129.
24. Shokrieh, M. M.; Hosseinkhani, M. R.; Naimi-Jamal, M. R.; Tourani, H. *Polym. Test.* **2013**, *32*, 45.
25. Chiu, F. C.; Huang, I. N. *Polym. Test.* **2012**, *31*, 953.
26. Kuila, T.; Khanra, P.; Mishra, A. K.; Kim, N. H.; Lee, J. H. *Polym. Test.* **2012**, *31*, 282.
27. Kuila, T.; Bose, S.; Mishra, A. K.; Khanra, P.; Kim, N. H.; Lee, J. H. *Polym. Test.* **2012**, *31*, 31.
28. Ecoflex F blend C1200 Data sheet, BASF. http://www.plasticsportal.net/wa/plasticsEU~tr_TR/function/conversions:/publish/common/upload/biodegradable_plastics/Ecoflex_F_Blend_C1200.pdf
29. Technical data sheet-xGnP® Graphene Nanoplatelets Grade M Characteristics, XG Sciences Inc. http://xgsciences.com/wp-content/uploads/2012/10/10-15-13_xGnP-M_Data-Sheet.pdf
30. Weir, W. B. Automatic measurement of complex dielectric constant and permeability at microwave frequencies. *Proc. IEEE* **1974**, *62*, 33.
31. Li, Y.; Zhu, J.; Wei, S.; Ryu, J.; Sun, L.; Guo, Z. *Macromol. Chem. and Phys.* **2011**, *212*, 1951.
32. Narimissa, E.; Gupta, R. K.; Choi, H. J.; Kao, N.; Jollands, M. *Polym. Compos.* **2012**, *33*, 1505.
33. Kashi, S.; Gupta, R. K.; Baum, T.; Kao, N.; Bhattacharya, S. N. *Mater. Des.* **2016**, *95*, 119.
34. El Achaby, M.; Arrakhiz, F. E.; Vaudreuil, S.; el Kacem Qaiss, A.; Bousmina, M.; Fassi-Fehri, O. *Polym. Compos.* **2012**, *33*, 733.
35. Murariu, M.; Dechief, A. L.; Bonnaud, L.; Paint, Y.; Gallos, A.; Fontaine, G.; Bourbigot, S.; Dubois, P. *Polym. Degrad. Stabil.* **2010**, *95*, 889.
36. Gao, C.; Zhang, S.; Wang, F.; Wen, B.; Han, C.; Ding, Y.; Yang, M. *ACS Appl. Mater. Interfaces* **2014**, *6*, 12252.
37. Pötschke, P.; Fornes, T.; Paul, D. *Polymer* **2002**, *43*, 3247.
38. Di, Y.; Iannace, S.; Di Maio, E.; Nicolais, L. *J. Polym. Sci. Part B: Polym. Phys.* **2003**, *41*, 670.
39. Narimissa, E.; Gupta, R. K.; Kao, N.; Choi, H. J.; Jollands, M.; Bhattacharya, S. N. *Polym. Eng. Sci.* **2014**, *54*, 175.
40. Ray, S. S.; Bousmina, M.; Okamoto, K. *Macromol. Mater. Eng.* **2005**, *290*, 759.
41. Ko, S. W.; Gupta, R. K.; Bhattacharya, S. N.; Choi, H. J. *Macromol. Mater. Eng.* **2010**, *295*, 320.
42. Gu, S. Y.; Ren, J.; Dong, B. *J. Polym. Sci. Part B: Polym. Phys.* **2007**, *45*, 3189.
43. Song, Y. S.; Youn, J. R. *Carbon* **2005**, *43*, 1378.
44. Bhattacharya, S. N.; Gupta, R. K.; Kamal, M. R. Polymeric Nanocomposites, Theory and Practice; Carl Hanser Verlag GmbH & Co. KG, **2008**; pp 147–163.
45. Dealy, J.; Plazek, D. *Rheol. Bull.* **2009**, *78*, 16.
46. Lee, K. M.; Han, C. D. *Polymer* **2003**, *44*, 4573.
47. Gelfer, M. Y.; Burger, C.; Chu, B.; Hsiao, B. S.; Drozdov, A. D.; Si, M.; Rafailovich, M.; Sauer, B. B.; Gilman, J. W. *Macromolecules* **2005**, *38*, 3765.
48. Kelarakis, A.; Yoon, K.; Somani, R. H.; Chen, X.; Hsiao, B. S.; Chu, B. *Polymer* **2005**, *46*, 11591.
49. Kelarakis, A.; Giannelis, E. P. *Polymer* **2011**, *52*, 2221.
50. Shenoy, A. V. In Rheology of Filled Polymer Systems; Springer Science & Business Media, **1999**; Chapter 6. p. 252–255.
51. Gu, S. Y.; Ren, J.; Wang, Q. F. *J. Appl. Polym. Sci.* **2004**, *91*, 2427.
52. Carreau, P. J. Transactions of the Society of Rheology (1957–1977) **1972**, *16*, 99.
53. Ren, J.; Krishnamoorti, R. *Macromolecules* **2003**, *36*, 4443.